INVESTIGATING FLOOD-VEGETATION INTERACTIONS THROUGH REMOTE SENSING AND MODELING

Elizabeth M. Prior[1], Jonathan A. Czuba[1], Thomas J. Pingel[2], Valerie A. Thomas[3], Randolph H. Wynne[3], W. Cully Hession[1]

1. Department of Biological Systems Engineering, Virginia Tech
2. Department of Geography, Virginia Tech
3. Department of Forest Resources and Environmental Conservation, Virginia Tech

---

Abstract

Understanding floodplain surface water processes is important due to the ever-increasing risk of high flow events and flooding, but has always been challenging because of spatiotemporal variability. One of the most elusive parameters to quantify is how vegetation obstructs flow by introducing friction into the system, also known as roughness. By utilizing unoccupied aerial systems lidar remote sensing and two-dimensional hydrodynamic modeling, my research aims to better understand how roughness varies with water depth, seasonally and in between individual flood events. For this presentation, I detail the progress I have made on this study: field data collection, lidar data collection, lidar corrections, creating the final digital elevation model (DEM), and creating a hydrodynamic model. Future steps demonstrate how I will use the hydrodynamic model to compare to my field data, along with how I plan to use the lidar data to represent floodplain vegetation roughness.

1. Introduction

1.1 Motivation

High flow events and flooding are expected to increase in both frequency and magnitude due to global climate change (Groisman et al., 2001; Hirabayashi et al., 2013; Karl et al., 2008). Thus, understanding surface water processes is essential for accurate flood predictions. One of the most variable physical parameter is roughness by vegetation resisting flow, also known as Manning's roughness coefficient (n), which decreases velocities and increases flood depths (Hession and Curran, 2013). Vegetation along streams is difficult to measure because of variability in time and space. Vegetative roughness is not accurately quantified or monitored in research or industry due to lack of geospatial data integration, resulting in inept flood peak estimations leading to inadequate flood mitigation or costly overpreparation.

1.2 Research objective

These shortcomings will be addressed by using unoccupied aerial systems (UAS) to investigate the impact that vegetation seasonality, heterogeneity and structure have on floodplain roughness through the coupling of remote sensing with flood modeling. This will be done by utilizing several tools to study flood-vegetation interactions including, two-dimensional (2D) hydrodynamic modeling with inputs from light detection and ranging (lidar).

1.3 Background

By utilizing lidar and the UAS platform, we are able to fully account for riparian vegetation variability in space (across the floodplain and vertically through the vegetation structure) and

time (seasonal die-off, scour and post-flood herbaceous vegetation flattening). Lidar utilizes near infrared light pulses that are then deflected off objects back to the sensor. The sensor records how long it takes the pulse to return, and then calculates elevation by using the speed of light. This then creates a 3D point cloud, that penetrates the canopy and detect the ground.

1.4 Initial results

Preliminary data have shown the benefits of using UAS lidar data to derive spatial distributions of roughness or Manning's n in raster form for input to hydrodynamic models. This has been published in a peer-reviewed journal (Prior et al., 2021). This initial study did not account for vegetation health, roughness alternations between floods or between seasons, or depth-dependent roughness. The study utilized one point cloud and compare modeled results to seven flood events.

2. Methods

2.1 Field site

All data has been collected at the Virginia Tech (VT) Stream Research, Education, and Management (StREAM) Lab (Figure 1). This outdoor laboratory is a 2.1 km restored section of Stroubles Creek used for interdisciplinary research. This site offers the desired riverscape complexity and long-term stage data, thus allowing for model validation and calibration.

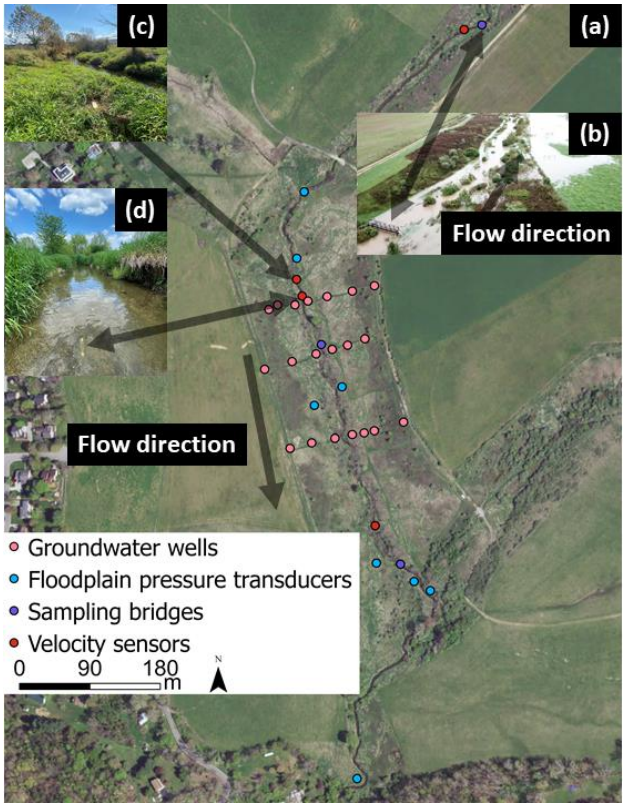

Figure 1. (a) Map of the VT StREAM Lab. (b) View of the first sampling bridge during a flood event, (c) floodplain velocity sensor, (d) in-stream velocity sensor.

2.2 Field data

At StREAM Lab, there is *in-situ* monitoring to assess the long-term effects of the stream restoration completed in 2010. There are three monitoring bridges where stage and water quality parameters are continuously measured every 15 minutes (Figure 1b). There are eighteen groundwater wells with pressure transducers and eight floodplain pressure transducers (HOBO, Onset Computer Corporation, Bourne, MA, USA) measuring water elevations every 15 minutes (Figure 1). Sontek-IQ Plus uplooking acoustic Doppler velocity meters (Sontek—a Xylem brand, San Diego, CA, USA) were deployed throughout the stream, with three deployed in the channel (Figure 1d) and one in the floodplain (Figure 1c). The velocity sensors, placed in the

thalweg, recorded an average velocity profile over a duration of 2 min and reported this average velocity profile every 5 min. Vertically averaged velocity was estimated by fitting a logarithmic curve (Garcia, 2008; Keulegan, 1938) to the profile and then average velocity was determined from the curve fit. This was done to account for unmeasured regions in the velocity profile, such as near the bed and at the water surface (Garcia, 2008). Lastly, when possible the extent of the flood was flagged and surveyed to determine water surface elevations at the peak flow throughout the study area. These field data were used to calibrate (velocity sensors), validate (wells), and compare (flood extents) to the hydrodynamic model.

2.3 Lidar data

The UAS system utilized for lidar surveys was a Vapor35 (AeroVironment, Simi Valley, CA, USA) with a YellowScan Surveyor Core lidar unit (Monfeerier-sur-Lez, France). The lidar unit consists of a Velodyne VLP-16 laser scanner (Velodyne, San Jose, CA, USA) and a GNSS-inertial Trimble APPLANIX APX-15 (Trimble, Richmond Hill, ON, Canada). To plan and conduct Vapor35 flights, we used the wePilot1000 flight control system and the weGCS ground control system software (weControl SA, Courtelary, Switzerland). The lidar flights were flown at a 30 m altitude, with 20 m flight-line spacing, which was recommended by YellowScan staff for optimum point spacing and density.

The YellowScan system is ultralight (2.1 kg) which is the allowable payload limit for the Vapor35. The lidar system can record two returns per pulse and uses a wavelength of 905 nm. The Velodyne VLP-16 and the APPLANIX unit allow for one button data acquisition. After the flight, data was corrected using a local CORS base station, and was outputted into a LAS file format in UTM zone 17N.

2.3.1 Lidar corrections

On initial inspection of the lidar data, misalignment in both the vertical (z) and horizontal (xy) directions were apparent when comparing scanlines from each flight (Figure 2b and 2c). Each flight consists of four to six scans that are then merged together to create the final point cloud. These misalignments were most apparent when inspecting sampling bridges, but are also present at other human-made objects in the floodplain, such as fence posts, gates, the weather station, and cars.

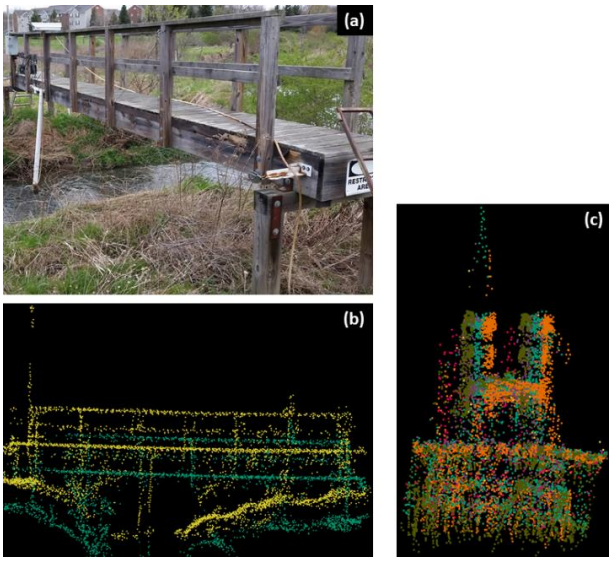

Figure 2. Lidar misalignment demonstrated at two sample bridges with the different color point clouds representing different scanlines within one flight. (a) image of the first sampling bridge, (b) vertical misalignment occurring at the first sampling bridge between two scans, (c) horizontal misalignment occurring at the second sampling bridge between four scans.

To correct these misalignments, the CloudCompare software (https://www.danielgm.net/cc/) was used to fix the misalignments by aligning to 2018 Virginia Geographic Information Network (VGIN) lidar and surveyed bridge points. First, a minimum filter was applied to our data and to the VGIN

lidar. Once both the minimum filtered points were produced, iterative closest point (ICP) was used to minimize the difference between the two clouds of points. This produces a transformation matrix, which was then applied to our original point cloud. This shifted the point cloud to be more aligned with the VGIN lidar data. Manual adjustment was then done to better align with the surveyed bridge points. This was then done for each scan, until all scans were aligned and merged (Figure 3a).

Next, the point cloud was then passed through a Python code that utilized the Simple Morphological Filter (SMRF) to classify ground points (Pingel et al., 2013). SMRF was modified to better account for the high density of points, along with the local topography (window size = 2, slope threshold = 0.15, elevation threshold = 0.1, elevation scaler = 1.25 and cell size = 0.5). Along with classifying ground, vegetation was classified as low, medium and high by utilizing the above ground height that was previously calculated by SMRF (low vegetation < 1 m, medium vegetation between 1 m and 3 m, high vegetation > 3 m). These vegetation height thresholds can easily be changed in the future. A portion of the classified point cloud can be seen in Figure 3b. The points were then used to create a digital elevation model (DEM).

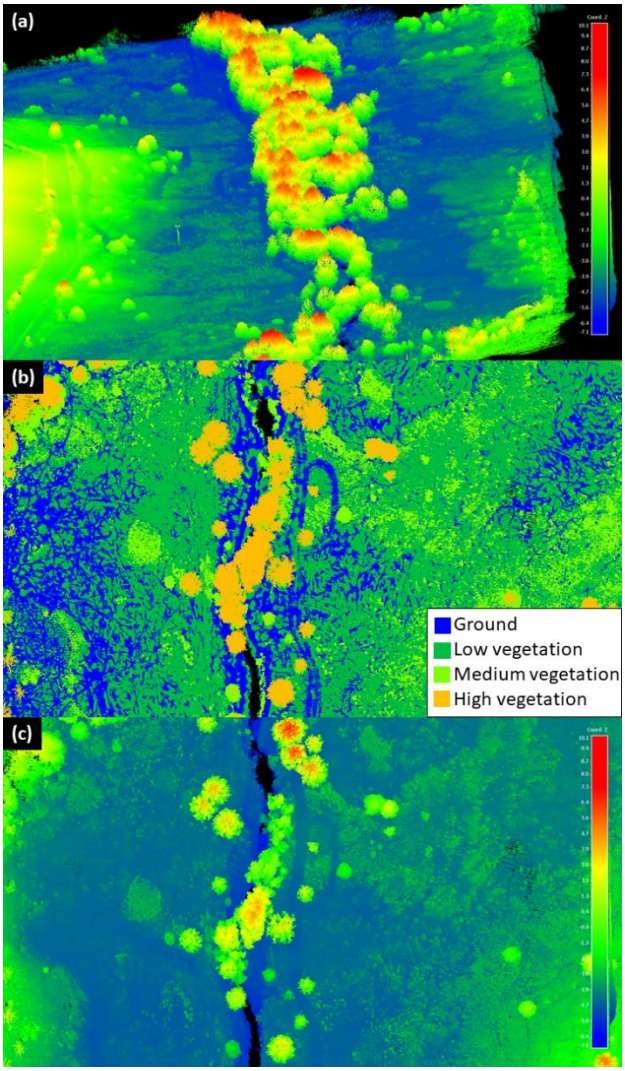

Figure 3. Final point cloud colored by Z coordinate value (a and c), and classification (b).

2.3.2 Final DEM

The point cloud file was then imported into ArcGIS Pro (version 2.9.2). It was filtered to just include the points classified as ground (Figure 4b). The ground points were then used to create a DEM raster by using the "LAS Dataset to Raster" tool, where the interpolation type was set to binning, cell assignment was set to nearest and void fill method was set to natural neighbor. Raster size was set to 15 cm.

Next, bathymetric cross-sections surveyed all along the stream were then used to create a raster of stream bathymetry using the "Topo to Raster." The bathymetry raster and the DEM raster were then combined using the "Mosaic to New Raster" tool (Figure 4d).

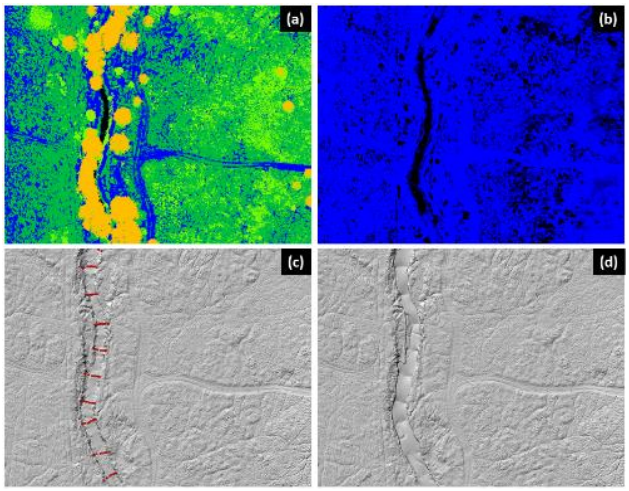

Figure 4. Process of going from a classified point cloud (a) to the final DEM (d) by isolating just the ground points (b), creating a surface from the ground points and utilizing surveyed cross-sections of bathymetry (c).

2.4 Model creation

Next, a hydrodynamic model was created in Hydrologic Engineering Center's River Analysis System (HEC-RAS). First, the DEM raster was imported in as a new terrain. A shapefile outlining the expected 2D flow area was created in ArcGIS Pro and imported into HEC-RAS. The 2D flow area mesh was created with 1 m cells. The boundary conditions were then created, with the upstream boundary condition being a flow hydrograph of flows that we have observed in the field, and the downstream boundary condition being normal depth with a friction slope of 0.0025.

A shapefile of the break lines and the refinement regions were created in ArcGIS Pro and imported into HEC-RAS (Figure 5). The break lines represent where there are natural changes in the topography (i.e. from inset floodplain to the main floodplain). The refinement region allows the user to create a finer mesh. This was done for the main channel, so that the 2D mesh in the channel consisted of 0.5 m cells.

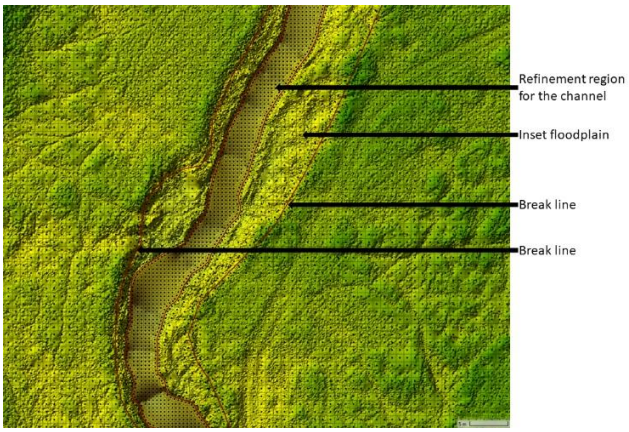

Figure 5. Zoom in of model and differing areas.

A raster of roughness values was created in ArcGIS Pro and was imported in as landcover. Only two roughness values were used: 0.04 for the channel and 0.5 for the floodplain, which were previously determined through model calibration in (Prior et al., 2021). Lastly, reference points were imported into HEC-RAS as a shapefile containing all locations of the field sensors (Figure 6). Having reference points makes it easier to output modeled results exactly where the field sensors are located.

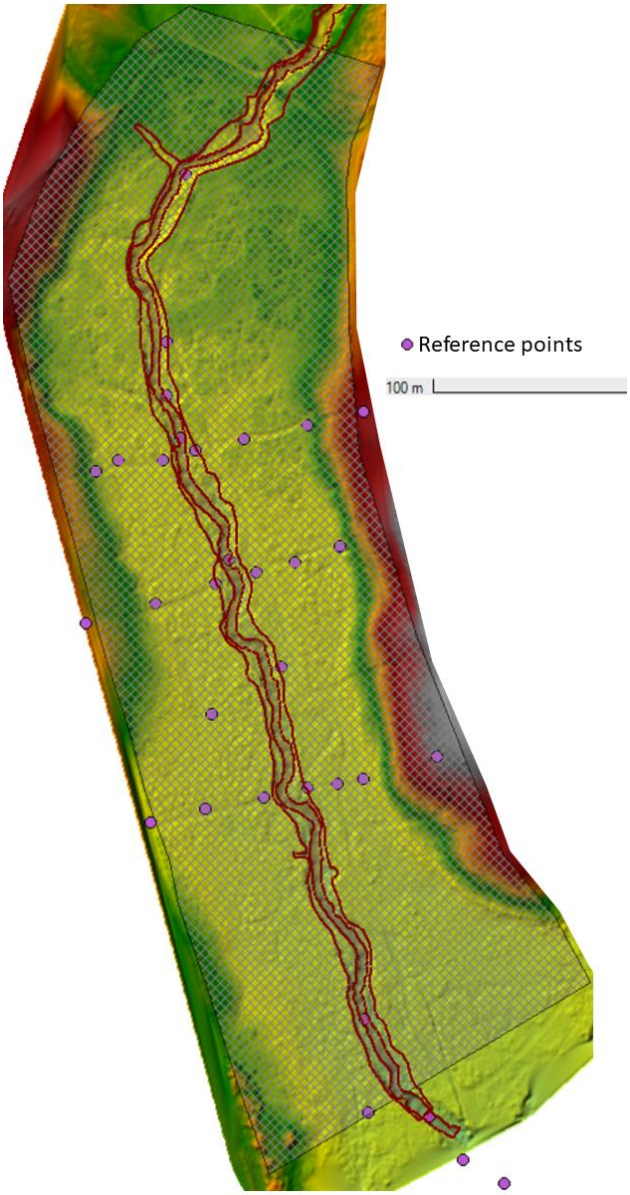

Figure 6. Model overview with reference areas showing where in-field sensors are located, and the gray grid showing the 2D flow area.

5. Future steps

Creating this model was a fundamental step in my research since it will now be used in all proceeding steps and analysis. The first project using this model will be to determine if DEM resolution and the nominal grid size of the 2D flow area greatly affect model outputs. These model outputs include flood extent, velocity and water surface elevation. This work will allow me to determine the most appropriate resolution for the DEM and 2D flow are, both of which will be used in future steps.

I also plan to utilize the entire point cloud to estimate roughness, and not just simplify the lidar information into a 2D space such as a raster. Equations developed by (Fathi-Maghadam and Kouwen, 1997; Kouwen, 1988; Kouwen and Li, 1980) will be applied to the point cloud directly surrounding the second velocity sensor located in the channel. Lidar will provide vegetation height information, while the normal depth and the velocity will be provided by the velocity sensor. Separately, I will also apply machine learning techniques to the point cloud as the water surface elevation changes to see if machine learning can output a similar roughness value to the velocity sensor data. Comparing machine learning results to the established equations will better inform us on how roughness changes with water surface elevation (i.e. depth-dependent roughness), and how the point cloud can help estimate these values.

Once this is better understood, roughness rasters that represent roughness at various water surface elevations can be created and inputted into the 2D HEC-RAS model. Additionally, the DEM resolution along with the 2D flow area resolution will have been better constrained by the first study. These depth specific roughness rasters will further allow us to better understand and model depth-dependent roughness.

Additionally, interseasonal roughness can be further investigated since my lab group has been collecting seasonal lidar data since 2017. I can determine what affect vegetation die-off from seasonal change has on flood extent, water surface elevations and velocities through evaluation of the field data and hydrodynamic modeling. Another potential project could be to investigate how roughness changes between

floods due to scour and flattening of herbaceous vegetation. I would need to collect lidar before and immediately after a flood event to best represent current conditions. This has yet to be done since we are constrained to UAS flights during specific weather conditions.

My research will evaluate the effects that water depth and seasonality have on vegetative roughness. Once vegetation roughness is better understood, new connections can be established on how ecohydraulics may affect relationships among sediment transport, biota habitat and surface water hysteresis. Additionally, this research will better constrain best practices for hydrodynamic modeling, which has societal implications for forecasting flood events. Other beneficiaries include infrastructure resiliency, stream restoration, riparian buffer zone design and watershed management planning. Thus, this work will not only improve modeling efforts of floodplains but aid management decisions in mitigating flood risks.

References

Fathi-Maghadam, M., Kouwen, N., 1997. Nonrigid, nonsubmerged, vegetative roughness on floodplains. Journal of Hydraulic Engineering 123, 51–57. https://doi.org/10.1061/(ASCE)0733-9429(1997)123:1(51)

Garcia, M., 2008. Chapter 2 Sediment Transport and Morphodynamics, in: Sedimentation Engineering: Processes, Measurements, Modeling, and Practice. American Society of Civil Engineers.

Groisman, P.Ya., Knight, R.W., Karl, T.R., 2001. Heavy Precipitation and High Streamflow in the Contiguous United States: Trends in the Twentieth Century. Bulletin of the American Meteorological Society 82, 219–246. https://doi.org/10.1175/1520-0477(2001)082<0219:HPAHSI>2.3.CO;2

Hession, W., Curran, J., 2013. 12.6 The Impacts of Vegetation on Roughness in Fluvial Systems, in: Treatise on Geomorphology. Elsevier, pp. 75–93.

Hirabayashi, Y., Mahendran, R., Koirala, S., Konoshima, L., Yamazaki, D., Watanabe, S., Kim, H., Kanae, S., 2013. Global flood risk under climate change. Nature Climate Change 3, 816–821. https://doi.org/10.1038/nclimate1911

Karl, T.R., Meehl, G.A., Miller, C.D., Hassol, S.J., Waple, A.M., Murray, W.L., 2008. Weather and climate extremes in a changing climate. US Climate Change Science Program.

Keulegan, G.H., 1938. Laws of turbulent flow in open channels. Journal National Bureau of Standards, Research Paper 1151 21, 35.

Kouwen, N., 1988. Field estimation of the biomechanical properties of grass. Journal of Hydraulic Research 26, 559–568. https://doi.org/10.1080/00221688809499193

Kouwen, N.N., Li, R.-M., 1980. Biomechanics of vegetative channel linings. Journal of the Hydraulics Division 106.

Pingel, T.J., Clarke, K.C., McBride, W.A., 2013. An improved simple morphological filter for the terrain classification of airborne LIDAR data 77, 21–30. https://doi.org/10.1016/j.isprsjprs.2012.12.002

Prior, E.M., Aquilina, C.A., Czuba, J.A., Pingel, T.J., Hession, W.C., 2021. Estimating Floodplain Vegetative Roughness Using Drone-Based Laser Scanning and Structure from Motion Photogrammetry. Remote Sensing 13, 2616.